ACS APPLIED ENERGY MATERIALS

www.acsaem.org Article

Ultralong-Life Quinone-Based Porous Organic Polymer Cathode for High-Performance Aqueous Zinc-Ion Batteries

Onur Buyukcakir,*[,◆] Recep Yuksel,[◆] Ferit Begar, Mustafa Erdogmus, Madi Arsakay, Sun Hwa Lee, Sang Ouk Kim, and Rodney S. Ruoff*

Cite This: *ACS Appl. Energy Mater.* 2023, 6, 7672−7680 Read Online

ACCESS | Metrics & More | Article Recommendations | Supporting Information

ABSTRACT: We synthesized and studied a redox-active quinone-based porous organic polymer (rPOP) and found ultralong cycle life: it is a promising organic cathode for aqueous zinc-ion batteries (ZIBs). It has high physicochemical stability and enhanced intrinsic conductivity from its fused-aromatic conjugated skeleton. rPOP's high porosity allows for efficient Zn^{2+} infiltration through the pores during charging−discharging cycles and contributes to the efficient utilization of redox-active quinone units. It delivers a specific capacity of 120 mAh g^{-1} at a current density of 0.1 A g^{-1} with a flat and long discharge plateau, which is critically important to provide a stable voltage output. It provides ultralong cycle life at a current density of 1.0 A g^{-1} for 1000 and at 2.0 A g^{-1} for 30 000 cycles, with initial capacity retention of 95 and 66%, respectively. The co-insertion (Zn^{2+} and H^+) charge storage mechanism was investigated using various electrochemical measurements and ex/in situ structural characterization techniques, and is explained herein. These findings contribute to a better understanding of the structure−property relationship for rPOP and open a new avenue for new organic cathode materials for high-performance next-generation aqueous batteries.

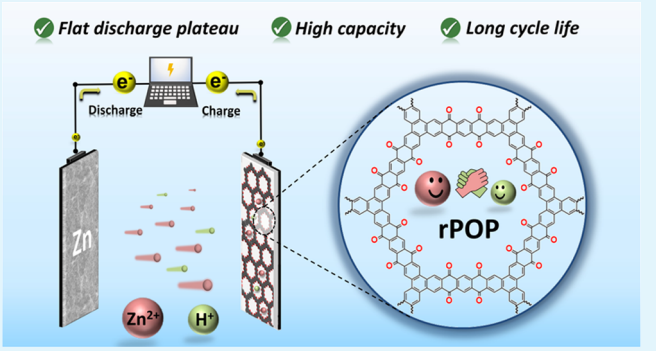

KEYWORDS: *porous organic polymers, zinc-ion batteries, organic cathode, long cycle life, energy storage*

INTRODUCTION

The need for energy storage systems with high performance, environmental benignity, and low cost has been snowballing due to ever-increasing energy demand.[1] Meanwhile, the increasing apprehension about environmental pollution and economic concerns increase the necessity for the utilization of renewable energy to attain a sustainable society.[2] Although rechargeable lithium-ion batteries (LIBs) have been extensively used to power portable electronics and electrical vehicles (EVs) in the past decades, the limited lithium sources and safety issues arising from the usage of flammable organic electrolytes restrain their usage for grid-level energy storage systems.[3−6] Therefore, there is an urgent need for the development of alternative battery technologies to complement LIBs, particularly in large-scale applications.[7,8] In this respect, rechargeable aqueous zinc-ion batteries (ZIBs) have attracted considerable attention compared to other monovalent (Li^+, Na^+, and K^+) and multivalent (Mg^{2+}, Ca^{2+}, and Al^{3+}) metal-ion batteries due to the nature of the zinc anode that offers high theoretical capacity (820 mAh g^{-1} and 5855 mAh cm^{-3}), low redox potential (−0.76 V vs standard hydrogen electrode (SHE)), aqueous electrolyte compatibility, safety, and economic viability.[9−11] New cathodes offering high capacity and long cycle life play a crucial role in developing high-performance rechargeable aqueous zinc-ion batteries (ZIBs).

The research on aqueous ZIBs mainly focuses on developing a suitable cathode material that can reversibly accommodate Zn^{2+} ions.[12−14] To date, several inorganic materials have been proposed as cathode materials to build high-performance ZIBs. Most of them are mainly based on transition-metal oxides (manganese, vanadium, and molybdenum oxides),[15−17] spinel-type materials,[18] and Prussian blue analogues.[19] Unfortunately, these inorganic cathodes suffer from low capacity, gradual capacity fading, and poor cycle life owing to dissolution in the electrolyte, significant volumetric change, and unstable phase transition during the discharge/charge process. In addition, the applicability of some of these conventional inorganic cathode materials is constrained by their high cost and toxicity due to the nature of the metal they contain.[20] Researchers have recently recognized the potential of redox-active organic

Received: May 8, 2023
Accepted: June 15, 2023
Published: June 29, 2023

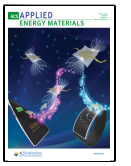

compounds as alternatives for inorganic electrode materials due to their sustainability, cost, and versatility in molecular design.[21−25] Among various organic groups, carbonyl-containing organic compounds, such as calix[4]quinone,[26] phenanthraquinone,[27] p-chloranil,[28] and 1,4,5,8-naphthalene diimide,[29] show promising redox activity in rechargeable aqueous ZIBs and reversibly host Zn^{2+} ions by coordination reactions. Nevertheless, the high solubility of their discharged products in aqueous electrolytes and their poor conductivity hinder their electrochemical performances regarding cycle stability and rate capability. Although the polymerization or the covalent attachment of organic redox-active units to conductive polymer chains (or conductive carbons) can reduce their solubility and contribute to their electrical conductivity, they have suffered from polymer aggregation during repeated electrochemical cycles.[30−32] This gradual aggregation inhibits the effective diffusion of Zn^{2+} ions into the interior redox-active site, which is buried deep within the stacked layers of polymer chains and slows down Zn^{2+} infiltration. It is, therefore, necessary to design and produce new types of cathode materials that can outperform the electrochemical performance of existing inorganic and organic materials to construct high-performance ZIBs.

Porous organic polymers (POPs), a class of porous materials constructed by covalently linking organic components to form polymeric networks, have distinct chemical and physical properties, including variable pore size, a large surface area, and excellent physicochemical stability.[33,34] Unlike small redox-active organic compounds, POPs have an insoluble extended structure that reduces the risk of active components leaching into the electrolyte solution during the charging/discharging cycles. Moreover, easy structural tunability at the molecular level provides a unique opportunity to tailor their electrochemical features by utilizing different redox-active moieties. All of the above features make POPs promising electrode materials for metal-ion batteries, and they have recently been employed in energy storage systems[35,36] in addition to their traditional applications, which include gas capture,[37] catalysis,[38] sensing,[39] and molecular separation.[40] To date, several POPs, including subclasses of covalent organic frameworks (COFs),[41−43] covalent triazine frameworks (CTFs),[44,45] conjugated microporous polymers (CMPs),[46,47] and porous aromatic frameworks (PAFs),[48,49] have been investigated as electrode materials in monovalent (Li^+, Na^+, and K^+) metal-ion batteries, particularly for LIBs. However, studies on POP-based ZIBs are still in their infancy, and to date, only a few COFs and CMPs, which contain phenazine (PA-COF),[50] P3Q,[51] PHATN-t,[52] phenylamine (m-PTPA),[53] thiophene (DA-CCPs),[54] and quinone (HqTp,[55] TP-PTO-COF,[56] TAQ-BQ,[57] BT-PTO-COF,[58] CTF-TTPQ,[59] HAQ-COF,[60] and PPPA[61]) groups, have been reported as cathode materials in rechargeable aqueous ZIBs. Although these polymers have shown promising electrochemical results in terms of capacity and rate capability, there are still issues that need to be resolved, such as the need for complex additives (due to their low conductivity), short cycle life, and absence of a flat discharge plateau to provide a consistent and stable voltage output, all of which are detrimental for practical applications.[50,55,57] Therefore, designing new electrochemically active POPs and understanding their Zn^{2+} storage mechanism to achieve the desired electrochemical performance and cost benefits are still of great interest.

We describe a new quinone-functionalized redox-active porous organic polymer (rPOP) using a modified version of the Diels−Alder reaction between hexakis(bromomethyl)-benzene and 1,4,5,8-anthracenetetrone. The synthesized polymer was used as a cathode material in aqueous ZIBs. Benefiting from the rich redox-active carbonyl groups (quinone units), conjugated backbone, and permanently porous structure, it showed a high capacity of 120 mAh g^{-1} at a current density of 0.1 A g^{-1} with unprecedented long-term cycling stability with 66% capacity retention after 30 000 cycles at the current density of 2.0 A g^{-1}. In addition, plateaus for charge−discharge curves without a direct slope can offer a constant voltage output, and 68% of the rPOP's total capacity originates from a limited voltage range of only 0.6−1.0 V at the current density of 0.1 A g^{-1}. The charge storage mechanism and the redox chemistry between quinone groups and charge carriers Zn^{2+}/H^+ were studied in detail by electrochemical analyses and ex/in situ characterization techniques. This study emphasizes the significance of the structural properties of POPs used in this field and significantly expands our knowledge of the relationship between the structure and properties of organic cathode materials used in ZIBs.

RESULTS AND DISCUSSION

The synthesis routes for preparing rPOP and the model compound are depicted in Figure 1. To ensure the feasibility of

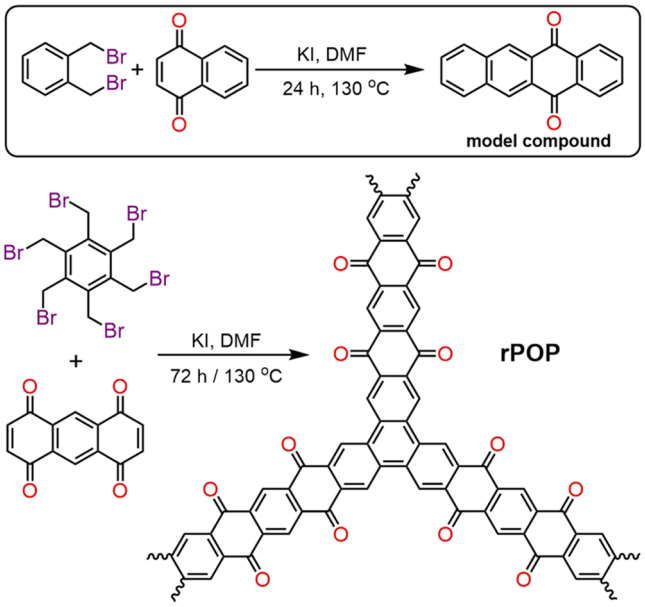

Figure 1. Schematic of the synthesis pathways for the model compound and rPOP.

the reaction and to discover the optimal conditions for polymerization, the model compound 5,12-naphthacenequinone was initially synthesized by treating naphthoquinone to a Diels−Alder reaction with, α,α'-dibromo-o-xylene. Following the optimized reaction protocol, the Diels−Alder reaction between hexakis(bromomethyl)benzene and the monomer, 1,4,5,8-anthracenetetrone, results in a high yield of the desired polymeric network, rPOP. Additional characterization details for the model compound and 1,4,5,8-anthracenetetrone are provided in the Supporting Information (^1H, ^{13}C NMR, and FT-IR spectra, Figures S1−S6).

https://doi.org/10.1021/acsaem.3c01163
ACS Appl. Energy Mater. 2023, 6, 7672−7680

Fourier transform infrared (FT-IR) spectroscopy initially confirmed the formation of the polymeric structure (Figure 2).

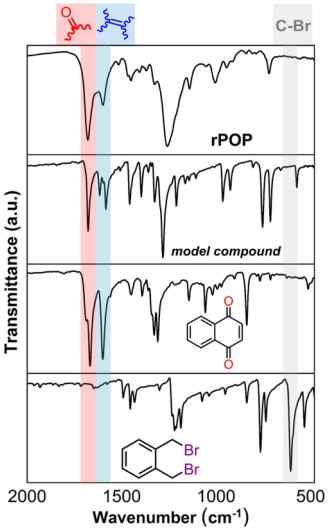

Figure 2. FT-IR spectra of the precursors, model compound, and rPOP.

The disappearance of C−Br stretching at about 600 cm^{-1} indicates the polymerization of hexakis(bromomethyl)benzene through the Diels−Alder reaction. The observed characteristic IR bands of C═O at 1700 cm^{-1} support the proposed structure of rPOP. To further investigate the chemical structure of the rPOP, solid-state cross-polarization magic angle spinning (CP/MAS) ^{13}C NMR spectroscopy was performed (Figure 3a). The broad resonance signal observed between 120 and 145 ppm was assigned to the carbon atoms of aryl groups, while the other resonance signal located at about 180 ppm belonged to the carbonyl carbon, which is consistent with the model compound. The elemental composition and chemical bonding nature of the model compound and rPOP were evaluated by X-ray photoelectron spectroscopy (XPS). The survey spectra of the model compound and rPOP show only the presence of C 1s and O 1s (Figure S7a,b). The high-resolution C 1s spectrum of rPOP can be deconvoluted into two peaks 284.6 and 287.3 eV, which can be attributed to carbon atoms in aromatic rings (C═C) and carbons bonded to oxygen atoms in the quinone moieties (C═O), respectively (Figure 3b). The high-resolution O 1s spectrum of rPOP was deconvoluted into two peaks with binding energies 531.6 and 533.4 eV, which can be, respectively, attributed to oxygen atoms of quinone units (C═O) and oxygen atoms in the moisture trapped in the pores of rPOP (Figure 3c). The high-resolution C 1s spectrum of the model compound is similar to the rPOP, which shows the peaks for the aromatic rings (C═C) and the quinone units (C═O) at 284.6 and 287.2 eV, respectively (Figure S7c). In the O 1s spectrum of the model compound, two sets of peaks with binding energies 531.5 and 533.3 eV were observed and attributed to C═O and moisture, respectively (Figure S7d). These results clearly verify the successful synthesis of rPOP.

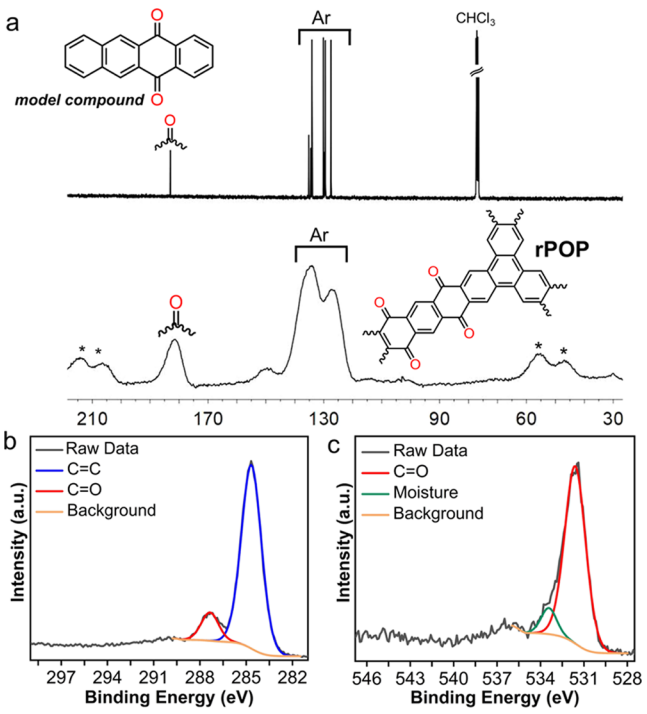

Figure 3. Structural characterization of rPOP. (a) Comparison of the solid-state ^{13}C NMR spectrum of rPOP and ^{13}C NMR spectrum of the model compound. High-resolution C 1s (b) and O 1s (c) XPS spectra of rPOP.

The observed broad features in the diffraction pattern of rPOP indicate the lack of long-range order of the polymeric network (Figure S8). The observed broad diffraction peak at ∼26° can be attributed to the ∼3.4 Å vertical $\pi-\pi$ stacking distance of rPOP layers. The particle morphology of rPOP was investigated using scanning electron microscopy (SEM) (Figure S9). SEM analysis reveals globular-like particles ranging in size from 200 to 300 nm. Energy-dispersive X-ray spectroscopy (EDX) was done to probe elemental mapping and revealed a homogeneous distribution of carbon and oxygen throughout the polymer (Figure S9). The rPOP shows remarkable thermal stability up to 400 °C (TGA data, Figure S10). The porosity of rPOP was assessed by adsorption−desorption isotherms using N_2 gas as adsorbate at 77 K (Figure S11a). The average value of 1.0 nm pore size distribution was obtained from the nonlocal density functional theory (Figure S11b). The relative pressure range determined using the Rouquerol plot (Figure S11c) was used to calculate the BET surface area of rPOP (BET plot, Figure S11d). The calculated BET surface area of rPOP is 737 $m^2\ g^{-1}$, and detailed porosity parameters of rPOP are summarized in Table S1. Notably, rPOP displays a significantly greater surface area compared to synthetically similar polymeric networks,[62] highlighting the impact of the synthetic process and the significance of monomer selection on the textural qualities of polymers.

The electrochemical performance of the rPOP cathode was tested in rechargeable aqueous ZIBs. The electrochemical performance of the rPOP cathode was investigated using Swagelok-type cells, which were assembled with Zn foil as the anode, a glass fiber membrane as a separator, and an aqueous 1 M $ZnSO_4$ solution as the electrolyte. Detailed procedures for the preparation of electrodes, construction of cells, and conditions for electrochemical tests are described in the Supporting Information. First, cyclic voltammetry (CV) measurements were performed to evaluate the reversibility of the insertion/de-insertion processes of ions. Figure 4a shows CV cycles collected at different scan rates (0.1−2.0 mV s^{-1}) in the potential range of 0.1−1.6 V. The CV cycles reveal a broad

https://doi.org/10.1021/acsaem.3c01163
ACS Appl. Energy Mater. 2023, 6, 7672−7680

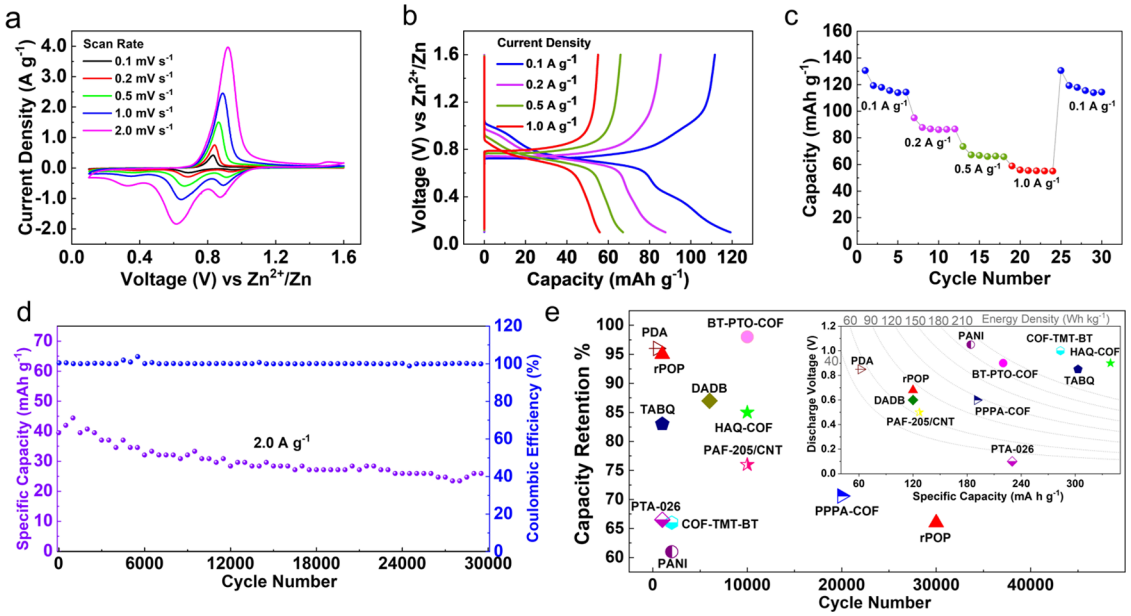

Figure 4. Electrochemical performance of the rPOP. (a) Cyclic voltammetry (CV) curves measured at different scan rates ranging from 0.1 to 2.0 mV s^{-1}. (b) Galvanostatic (dis-)charge profiles at various current densities. (c) Rate performance of rPOP at different current densities. (d) Long-term cycling stability of rPOP at a current density of 2.0 A g^{-1} up to 30 000 cycles. (e) Electrochemical performance (cycle number and capacity retention) comparison of the rPOP with previously reported organic cathodes for aqueous ZIBs. The inset shows the comparison plot of the energy density of rPOP at 0.1 A g^{-1} [HAQ-COF,[60] TABQ,[22] COF-TMT-BT,[63] BT-PTO-COF,[58] PANI,[64] PPPA-COF,[61] PTA-026,[65] PAF-205/CNT,[66] DADB,[67] PDA[68]].

oxidation peak at 0.95 V and three reduction peaks at 0.35, 0.68, and 0.83 V, which are related to the oxidation/reduction reactions occurring in the quinone moieties during the cations (de)insertion process. Similar CV patterns with small peak shifts and increasing cathode/anode peak currents at higher scan rates indicate good reversibility and the fast kinetics of cation insertion/de-insertion. The linear relationship between the peak current and the square root of the scan rates implies that the insertion/de-insertion of cations is governed by diffusion processes (Figure S12b).

Galvanostatic charge/discharge (GCD) measurements at various current densities were performed to explore the capacity and rate capabilities of the fabricated rPOP cathodes. Figure 4b,c depicts the discharge/charge profiles and rate performances of rPOP, respectively. rPOP has a specific capacity of 120 mAh g^{-1} at a current density of 0.1 A g^{-1} and shows specific capacities of 89, 69, and 58 mAh g^{-1} at current densities of 0.2, 0.5, and 1.0 A g^{-1}, respectively. These numbers demonstrate the high-rate capability of rPOP. While previously reported polymers, such as HqTp-COFs,[55] PA-COFs,[50] and TAQ-BQ,[57] revealed a typical sloping voltage profile, only a limited number of POPs have exhibited apparent charge–discharge plateaus. The observed plateaus for charge–discharge curves of rPOPs without an obvious nonzero sloping, being comparable to or more flat than Tp-PTO-COF[56] and BT-PTO-COF,[58] offers a stable voltage output, which should be helpful to practical applications. The major capacity contribution was observed between the voltage range of 1.0 and 0.6 V, which is about 68% of the total capacity of the rPOP at 0.1 A g^{-1}. The long-term cycling stability of rPOP was investigated at a current density of 1 A g^{-1} up to 1000 cycles with 95% of retention of its initial capacity (Figure S13a). It also maintains nearly 100% Coulombic efficiency (CE) throughout the cycles, proving the cells' long-term durability and high capacity retention. The cycling stability of the cells was also tested for ultralong cycling at a current density of 2.0 A g^{-1}. After 30 000 cycles, it maintains about 66% of the initial capacity (40 mAh g^{-1}) while preserving the high CE (Figures 4d and S13c). As summarized in Figure 4e and Table S2, rPOP shows slightly lower specific capacities compared to other recently reported polymeric cathodes. rPOP delivers reasonably high capacities compared to quinone containing small organic compound-based cathodes that suffer from high solubility of their discharged products in aqueous electrolytes and poor conductivity. Compared with the other organic cathodes (Figure 4e and Table S2), rPOP provides an ultralong cycle life with high capacity retention and a flat discharge plateau, which are particularly important for practical applications.

The electrochemical performance of 1,4,5,8-anthracenetetrone (monomer of rPOP) was tested in aqueous ZIBs as a cathode material. Figure S14a shows the CV cycle of 1,4,5,8-anthracenetetrone at a scan rate of 2.0 mV s^{-1} in the potential range of 0.1−1.6 V, which displays two oxidation peaks at 1.09 and 1.22 V and three reduction peaks at 0.48, 0.74, and 0.95 V, suggesting the oxidation/reduction reactions of quinone moieties. Compared to the rPOP cathode, 1,4,5,8-anthracenetetrone shows low specific capacities and rate performance (Figure S14b,c). It provides specific capacities of 57, 48, and 31 mAh g^{-1} at current densities of 0.1, 0.2, and 0.5 A g^{-1}, respectively. 1,4,5,8-Anthracenetetrone shows poor cycling stability compared to rPOP cathode and shows a specific capacity of only 28 mAh g^{-1} at a current density of 1.0 A g^{-1} over 1000 cycles with 82% capacity retention, which can be attributed to the solubility of its discharging product (Figure S14d). The dissolution of the rPOP electrode was tested by immersing the pristine, the discharged (0.1 V), and the charged (1.6 V) electrodes in 1 M $ZnSO_4$ electrolyte for 36 h. As depicted in Figure S15, the rPOP remained insoluble in the electrolyte even in a completely discharged state (0.1 V). rPOP

https://doi.org/10.1021/acsaem.3c01163
ACS Appl. Energy Mater. 2023, 6, 7672−7680

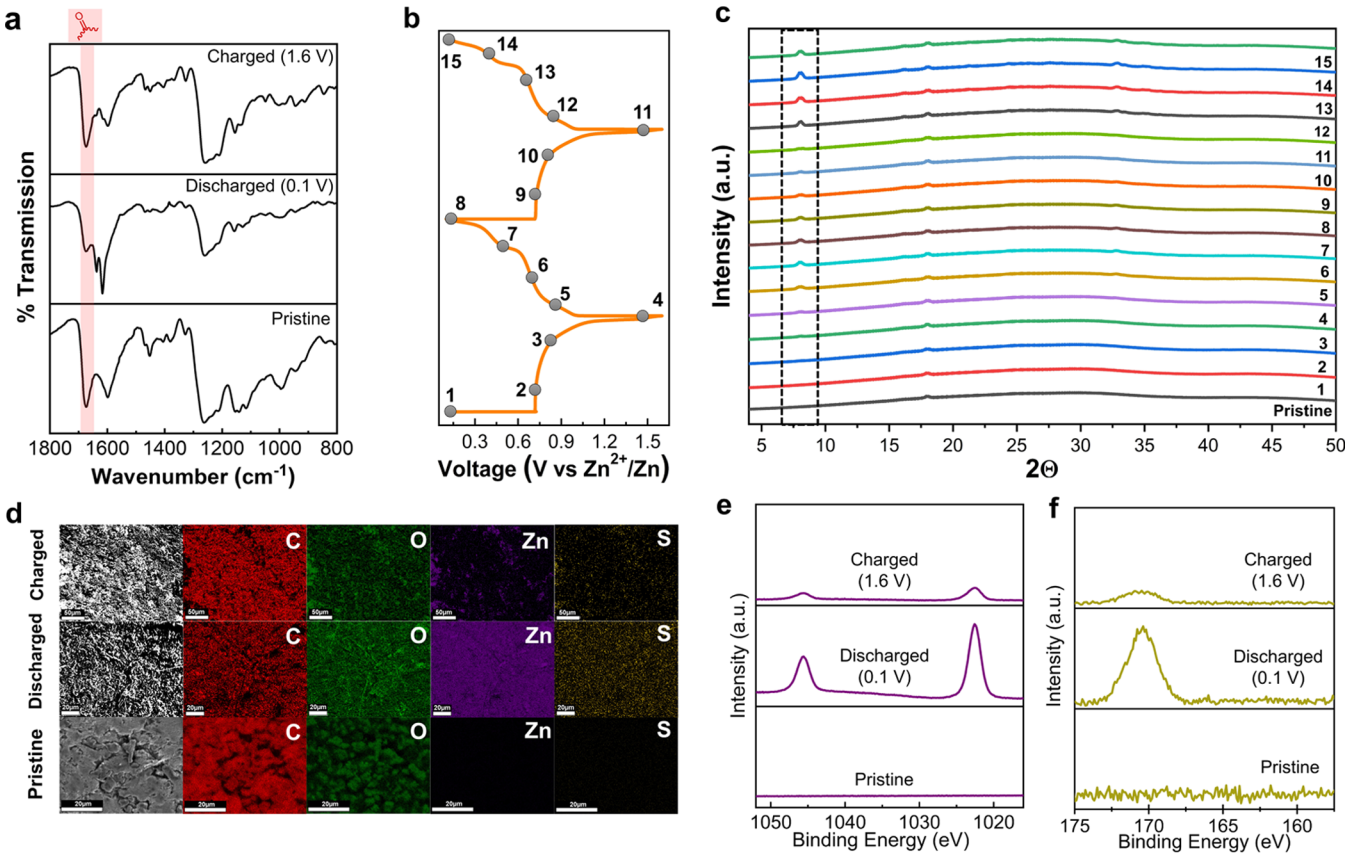

Figure 5. In/ex situ charge storage mechanism characterization of rPOP. (a) Ex situ FT-IR spectra of rPOP at pristine, charged, and discharged states. (b, c) In situ XRD analysis of rPOP recorded at various electrochemical states. (d) SEM images and EDX elemental mapping of pristine, charged, and discharged states for the elements of carbon (C), oxygen (O), zinc (Zn), and sulfur (S). Zn 2p (e) and S 2p (f) high-resolution XPS spectra of rPOP at pristine, charged, and discharged states.

cathodes have high electrochemical stability in rechargeable aqueous batteries.

The CV curves collected at different scan rates were also used to explore the electrochemical kinetic features of rPOP (Figure S12a). The distribution of faradaic/non-faradaic charge storage was calculated using the power law relationship ($i = av^b$, where a and b are adjustable parameters, i is the current, and v is the sweep rate). At $b = 0.5$, ionic diffusion is thought to be the only controlling factor in the charge/discharge process and implies an entirely diffusion-controlled charge storage mechanism (faradaic process), while a value of 1 indicates capacitive controlled charge storage (non-faradaic process). In this respect, it can be possible to estimate the kinetics of the electrode reactions from the b values, which are derived from the linear slope of $\log i$ vs $\log v$ (Figure S12c,d). The b value of the four distinctive redox peaks of rPOP at 0.35, 0.68, 0.83, and 0.95 V equals 0.94, 0.82, 0.75, and 0.82, respectively. The found b values suggest that rPOP is influenced by both diffusive and capacitive charge storage mechanisms. Although the b values higher than 0.8 indicate the larger contribution of the capacitive process over the diffusive-controlled charge storage mechanism, rPOP has lower b values than other quinone-containing POPs,[58,61] suggesting a more significant contribution of diffusion-controlled ion insertion.

The equation $[i(V) = k_1v + k_2v^{1/2}]$ proposed by Dunn and co-workers was used to calculate the faradaic and non-faradaic contributions quantitatively.[69] The equation divides the current into two components: capacitive current (k_1v) and diffusion-controlled current ($k_2v^{1/2}$) at a given voltage. The k_1 and k_2 values can be calculated by plotting $i/v^{1/2}$ vs $v^{1/2}$. At sweep rates of 0.1, 0.2, 0.5, 1.0, and 2.0 mV s^{-1}, the capacitive and diffusion-controlled contributions in all potential ranges were calculated and highlighted in the CV curves (Figure S16a−e). The corresponding capacitive contribution values for scan rates of 0.1, 0.2, 0.5, 1.0, and 2.0 mV s^{-1} are 28, 35, 46, 55, and 63%, respectively, as shown in Figure S16f, suggesting a rise in capacitive contribution with increasing discharge and charge rates. rPOP has a much more significant diffusive-controlled charge storage contribution than recently reported POP-based cathodes, like PA-COF,[50] G-Aza-CMP,[70] and HAQ-COF[60] (a detailed comparison is shown in Table S2).

The charge storage mechanism of the rPOP cathode was studied using a variety of ex situ and in situ measurements. FT-IR spectroscopy was used to investigate the active sites for ion accommodation in rPOP. As shown in Figure 5a, a significant decrease in the carbonyl stretching band (C═O, quinone moieties located at around 1700 cm^{-1}) was observed in the FT-IR spectrum of the discharged electrode (0.1 V), confirming that the quinone groups are responsible for the accommodation of ions. After charging to 1.6 V, the intensity of the carbonyl stretching peak was restored, and the charged electrode was thus back to the "pristine state", showing not only the removal of ions from the quinone units but also the reversible enolization of carbonyl moieties of rPOP during the charging and discharging.

https://doi.org/10.1021/acsaem.3c01163
ACS Appl. Energy Mater. 2023, 6, 7672−7680

Previous studies have shown that the electrochemistry at the cathode side does not only involve the Zn^{2+} ions but also that protons (H^+) function as charge carriers in slightly acidic electrolytes.[22,24,25,29,50,55,56,59] Accommodating H^+ ions by carbonyl units during the discharge process leads to a local pH increase, which promotes the precipitation of zinc hydroxy sulfate [$Zn_4SO_4(OH)_6{\cdot}nH_2O$] as a byproduct on the cathode surface. Thus, the reversible H^+ co-(de)insertion can be followed by the precipitation and dissolution of zinc hydroxy sulfate on the cathode surface during discharging and charging, respectively.

To probe the charge storage mechanism and follow the reaction byproducts, specifically [$Zn_4SO_4(OH)_6{\cdot}nH_2O$], an in situ XRD analysis was carried out. As shown in Figure 5c, the characteristic peaks of zinc hydroxy sulfate [$Zn_4SO_4(OH)_6{\cdot}5H_2O$] were observed in the in situ XRD spectra. The electrode shows relatively weak XRD signals in charged compared to discharged states, which clearly shows reversible precipitation and dissolution of $Zn_4SO_4(OH)_6{\cdot}5H_2O$ during the discharging and charging processes. The incomplete disappearance of the XRD signal belonging to $Zn_4SO_4(OH)_6{\cdot}5H_2O$ for the fully charged state suggests that a tiny quantity of $Zn_4SO_4(OH)_6{\cdot}5H_2O$ remains in the electrode after recharging. In addition, the SEM image of electrodes in the discharged state revealed tiny sheet-like structures, a typical morphology of $Zn_4SO_4(OH)_6{\cdot}5H_2O$, over the electrode surface (Figure 5d). EDX mapping analysis was carried out at the same region and revealed the uniform distribution of sulfur and zinc throughout the surface; however, their content significantly decreased after the charging process, which is attributed to the reversible precipitation and dissolution of $Zn_4SO_4(OH)_6{\cdot}5H_2O$ (Figure 5d). The EDX mapping of Zn and S elements shows tiny residual areas of $Zn_4SO_4(OH)_6{\cdot}5H_2O$, which is in good agreement with in situ XRD analysis.

Further evaluation of the reversible insertion/de-insertion of the Zn^{2+}/H^+ ions to rPOP cathodes was carried out using ex situ XPS analysis. The high-resolution Zn 2p and S 2p XPS spectra of the discharged electrode (0.1 V) show relatively stronger signals compared to the charged electrode (1.6 V), which can be ascribed to the formation and dissolution of $Zn_4SO_4(OH)_6{\cdot}5H_2O$, suggesting the reversible co-(de)-insertion of H^+ ions (Figure 5e,f). The S 2p spectrum of the charged electrode shows a weak signal, indicating that some sulfur remains in the electrode as a partial residue due to the incomplete dissolution of $Zn_4SO_4(OH)_6{\cdot}5H_2O$ during the charging progress. This result agrees with the XRD analysis and EDX mapping, suggesting the trapping of some H^+ ions after insertion. While rPOP shows good cyclic stability up to 30 000 cycles, the slight gradual capacity loss of rPOP can be attributed to the trapped H^+ ions, which stimulates the gradual accumulation of the $Zn_4SO_4(OH)_6{\cdot}5H_2O$ on the electrode surface.

Electrochemical measurements were performed to explore further the contribution of H^+ (de)insertion along with Zn^{2+} ions. A cell was assembled using 5×10^{-5} M H_2SO_4 (aq) electrolyte solution, which provides similar proton activity with $ZnSO_4$ (aq), in which rPOP and zinc foil was used as cathode and anode, respectively. From the CV curves, the 1 M $ZnSO_4$ (aq) reveals the merging of peaks, associated with pure Zn^{2+} and H^+ (de)insertion, as a broad oxidation peak at 0.95 V and three reduction peaks at 0.35, 0.68, and 0.83 V, indicating Zn^{2+} and H^+ co-(de)insertion process (Figure S17). However, comparing the CV curve areas of 1 M $ZnSO_4$ (aq) and 5×10^{-5} M H_2SO_4 (aq) indicates that Zn^{2+} dominates the charge storage process and H^+ partially contributes to the electrochemical performance. The cell prepared using 5×10^{-5} M H_2SO_4 (aq) electrolyte showed a 17% capacity contribution at a scan rate of 2.0 mV s^{-1} originating from H^+ co-(de)insertion.

CONCLUSIONS

rPOP containing redox-active quinone groups was proposed as a new organic cathode for rechargeable aqueous ZIBs. The Diels–Alder reaction approach was used to create rPOP under heavy-metal-free conditions. Its high porosity permits charge carriers (Zn^{2+}/H^+) to diffuse effectively through the pores during charging–discharging cycles, allowing for the efficient utilization of redox-active quinone units. The material's fused-aromatic conjugated skeleton also provides good physicochemical stability and increased intrinsic conductivity. These features of rPOP allow a superlong cycle life without compromising capacity and rate performance. It has a reversible specific capacity of 120 mAh g^{-1} at 0.1 A g^{-1} current density and cyclic stability up to 30 000 cycles (at 2.0 A g^{-1}) with good initial capacity retention (66%). The charge storage mechanism was thoroughly investigated, and the redox activity of quinone moieties and co-(de)insertion of Zn^{2+} and H^+ ions were found by electrochemical measurements and ex/in situ analysis. We suggest this study will open up new avenues for designing and synthesizing novel polymeric materials for developing high-performance rechargeable aqueous ZIBs.

ASSOCIATED CONTENT

Supporting Information

The Supporting Information is available free of charge at https://pubs.acs.org/doi/10.1021/acsaem.3c01163.

Detailed description of materials preparations including synthesis of monomers, model compound, and rPOP; additional structural and electrochemical characterization of rPOP; and XPS, XRD, TGA, gas sorption, and CV curves collected different sweep rates/electrolytes (PDF)

AUTHOR INFORMATION

Corresponding Authors

Onur Buyukcakir – *Department of Chemistry, Izmir Institute of Technology, Izmir 35430, Turkey;* orcid.org/0000-0003-4626-8232; Email: onurbuyukcakir@iyte.edu.tr

Rodney S. Ruoff – *Center for Multidimensional Carbon Materials, Institute for Basic Science (IBS), Ulsan 44919, Republic of Korea; Department of Chemistry, Ulsan National Institute of Science and Technology (UNIST), Ulsan 44919, Republic of Korea; School of Energy and Chemical Engineering and Department of Materials Science and Engineering, Ulsan National Institute of Science and Technology (UNIST), Ulsan 44919, Republic of Korea;* orcid.org/0000-0002-6599-6764; Email: rsruoff@ibs.re.kr

Authors

Recep Yuksel – *Department of Chemistry, Eskisehir Osmangazi University, Eskisehir 26040, Turkey;* orcid.org/0000-0001-8178-0165

https://doi.org/10.1021/acsaem.3c01163
ACS Appl. Energy Mater. 2023, 6, 7672–7680

Ferit Begar − *Department of Chemistry, Izmir Institute of Technology, Izmir 35430, Turkey;* orcid.org/0000-0002-2933-8350
Mustafa Erdogmus − *Department of Chemistry, Izmir Institute of Technology, Izmir 35430, Turkey*
Madi Arsakay − *Center for Multidimensional Carbon Materials, Institute for Basic Science (IBS), Ulsan 44919, Republic of Korea; Department of Chemistry, Ulsan National Institute of Science and Technology (UNIST), Ulsan 44919, Republic of Korea*
Sun Hwa Lee − *Center for Multidimensional Carbon Materials, Institute for Basic Science (IBS), Ulsan 44919, Republic of Korea;* orcid.org/0000-0003-1368-1274
Sang Ouk Kim − *Department of Materials Science and Engineering, Korea Advanced Institute of Science and Technology (KAIST), Daejeon 34141, Republic of Korea; National Creative Research Initiative Center for Multi-Dimensional Directed Nanoscale Assembly, Korea Advanced Institute of Science and Technology (KAIST), Daejeon 34141, Republic of Korea;* orcid.org/0000-0003-1513-6042

Complete contact information is available at: https://pubs.acs.org/10.1021/acsaem.3c01163

Author Contributions

◆O.B. and R.Y. contributed equally. The manuscript was written through contributions of all authors. All authors have given approval to the final version of the manuscript.

Notes

The authors declare no competing financial interest.

■ ACKNOWLEDGMENTS

This work was supported by the IBS (IBS-R019-D1), and subsequently by The Scientific and Technological Research Council of Turkey, TUBITAK Project (220Z024). The authors thank the Nuclear Magnetic Resonance Application and Research Center (NMRM-IZTECH) for the NMR experiments.

■ REFERENCES

(1) Dunn, B.; Kamath, H.; Tarascon, J.-M. Electrical Energy Storage for the Grid: A Battery of Choices. *Science* **2011**, *334*, 928−935.
(2) Yang, Z.; Zhang, J.; Kintner-Meyer, M. C. W.; Lu, X.; Choi, D.; Lemmon, J. P.; Liu, J. Electrochemical Energy Storage for Green Grid. *Chem. Rev.* **2011**, *111*, 3577−3613.
(3) Li, M.; Lu, J.; Chen, Z.; Amine, K. 30 Years of Lithium-Ion Batteries. *Adv. Mater.* **2018**, *30*, No. 1800561.
(4) Goodenough, J. B.; Park, K.-S. The Li-Ion Rechargeable Battery: A Perspective. *J. Am. Chem. Soc.* **2013**, *135*, 1167−1176.
(5) Kang, J.; Han, D.-Y.; Kim, S.; Ryu, J.; Park, S. Multiscale Polymeric Materials for Advanced Lithium Battery Applications. *Adv. Mater.* **2023**, *35*, No. 2203194.
(6) Kim, T.; Choi, S.; Ryu, J.; Kim, Y.; Lee, G.; Kim, B.-S.; Park, S. Surficial amide-enabled integrated organic anode−binder electrode for electrochemical reversibility and fast redox kinetics in lithium−ion batteries. *Appl. Surf. Sci.* **2022**, *601*, No. 154220.
(7) Ponnada, S.; Kiai, M. S.; Krishnapriya, R.; Singhal, R.; Sharma, R. K. Lithium-Free Batteries: Needs and Challenges. *Energy Fuels* **2022**, *36*, 6013−6026.
(8) Liu, K.; Liu, Y.; Lin, D.; Pei, A.; Cui, Y. Materials for lithium-ion battery safety. *Sci. Adv.* **2018**, *4*, No. eaas9820.
(9) Song, M.; Tan, H.; Chao, D.; Fan, H. J. Recent Advances in Zn-Ion Batteries. *Adv. Funct. Mater.* **2018**, *28*, No. 1802564.
(10) Zampardi, G.; La Mantia, F. Open challenges and good experimental practices in the research field of aqueous Zn-ion batteries. *Nat. Commun.* **2022**, *13*, No. 687.
(11) Yuksel, R.; Buyukcakir, O.; Seong, W. K.; Ruoff, R. S. Metal-Organic Framework Integrated Anodes for Aqueous Zinc-Ion Batteries. *Adv. Energy Mater.* **2020**, *10*, No. 1904215.
(12) Li, H.; Ma, L.; Han, C.; Wang, Z.; Liu, Z.; Tang, Z.; Zhi, C. Advanced rechargeable zinc-based batteries: Recent progress and future perspectives. *Nano Energy* **2019**, *62*, 550−587.
(13) Nam, K. W.; Park, S. S.; dos Reis, R.; Dravid, V. P.; Kim, H.; Mirkin, C. A.; Stoddart, J. F. Conductive 2D metal-organic framework for high-performance cathodes in aqueous rechargeable zinc batteries. *Nat. Commun.* **2019**, *10*, No. 4948.
(14) Zhang, Q.; Dou, Y.; He, Q.; Deng, S.; Huang, Q.; Huang, S.; Yang, Y. Emerging Carbonyl Polymers as Sustainable Electrode Materials for Lithium-Free Metal-Ion Batteries. *Energy Environ. Mater.* **2022**, *5*, 1037−1059.
(15) Zhong, C.; Liu, B.; Ding, J.; Liu, X.; Zhong, Y.; Li, Y.; Sun, C.; Han, X.; Deng, Y.; Zhao, N.; Hu, W. Decoupling electrolytes towards stable and high-energy rechargeable aqueous zinc−manganese dioxide batteries. *Nat. Energy* **2020**, *5*, 440−449.
(16) Hu, P.; Zhu, T.; Ma, J.; Cai, C.; Hu, G.; Wang, X.; Liu, Z.; Zhou, L.; Mai, L. Porous V2O5 microspheres: a high-capacity cathode material for aqueous zinc−ion batteries. *Chem. Commun.* **2019**, *55*, 8486−8489.
(17) Wan, F.; Niu, Z. Design Strategies for Vanadium-based Aqueous Zinc-Ion Batteries. *Angew. Chem., Int. Ed.* **2019**, *58*, 16358−16367.
(18) Yuan, X.; Sun, T.; Zheng, S.; Bao, J.; Liang, J.; Tao, Z. An inverse-spinel Mg_2MnO_4 cathode for high-performance and flexible aqueous zinc-ion batteries. *J. Mater. Chem. A* **2020**, *8*, 22686−22693.
(19) Zhang, L.; Chen, L.; Zhou, X.; Liu, Z. Towards High-Voltage Aqueous Metal-Ion Batteries Beyond 1.5 V: The Zinc/Zinc Hexacyanoferrate System. *Adv. Energy Mater.* **2015**, *5*, No. 1400930.
(20) Jia, X.; Liu, C.; Neale, Z. G.; Yang, J.; Cao, G. Active Materials for Aqueous Zinc Ion Batteries: Synthesis, Crystal Structure, Morphology, and Electrochemistry. *Chem. Rev.* **2020**, *120*, 7795−7866.
(21) Guo, Z.; Ma, Y.; Dong, X.; Huang, J.; Wang, Y.; Xia, Y. An Environmentally Friendly and Flexible Aqueous Zinc Battery Using an Organic Cathode. *Angew. Chem., Int. Ed.* **2018**, *57*, 11737−11741.
(22) Lin, Z.; Shi, H.-Y.; Lin, L.; Yang, X.; Wu, W.; Sun, X. A high capacity small molecule quinone cathode for rechargeable aqueous zinc-organic batteries. *Nat. Commun.* **2021**, *12*, No. 4424.
(23) Nam, K. W.; Kim, H.; Beldjoudi, Y.; Kwon, T.-w.; Kim, D. J.; Stoddart, J. F. Redox-Active Phenanthrenequinone Triangles in Aqueous Rechargeable Zinc Batteries. *J. Am. Chem. Soc.* **2020**, *142*, 2541−2548.
(24) Peng, H.; Xiao, J.; Wu, Z.; Zhang, L.; Geng, Y.; Xin, W.; Li, J.; Yan, Z.; Zhang, K.; Zhu, Z. N-Heterocycles Extended π-Conjugation Enables Ultrahigh Capacity, Long-Lived, and Fast-Charging Organic Cathodes for Aqueous Zinc Batteries. *CCS Chem.* **2022**, 1−13.
(25) Gao, Y.; Li, G.; Wang, F.; Chu, J.; Yu, P.; Wang, B.; Zhan, H.; Song, Z. A high-performance aqueous rechargeable zinc battery based on organic cathode integrating quinone and pyrazine. *Energy Storage Mater.* **2021**, *40*, 31−40.
(26) Zhao, Q.; Huang, W.; Luo, Z.; Liu, L.; Lu, Y.; Li, Y.; Li, L.; Hu, J.; Ma, H.; Chen, J. High-capacity aqueous zinc batteries using sustainable quinone electrodes. *Sci. Adv.* **2018**, *4*, No. eaao1761.
(27) Yang, B.; Ma, Y.; Bin, D.; Lu, H.; Xia, Y. Ultralong-Life Cathode for Aqueous Zinc-Organic Batteries via Pouring 9,10-Phenanthraquinone into Active Carbon. *ACS Appl. Mater. Interfaces* **2021**, *13*, 58818−58826.
(28) Kundu, D.; Oberholzer, P.; Glaros, C.; Bouzid, A.; Tervoort, E.; Pasquarello, A.; Niederberger, M. Organic Cathode for Aqueous Zn-Ion Batteries: Taming a Unique Phase Evolution toward Stable Electrochemical Cycling. *Chem. Mater.* **2018**, *30*, 3874−3881.

(29) Na, M.; Oh, Y.; Byon, H. R. Effects of Zn^{2+} and H^{+} Association with Naphthalene Diimide Electrodes for Aqueous Zn-Ion Batteries. *Chem. Mater.* **2020**, *32*, 6990−6997.
(30) Han, C.; Li, H.; Shi, R.; Zhang, T.; Tong, J.; Li, J.; Li, B. Organic quinones towards advanced electrochemical energy storage: recent advances and challenges. *J. Mater. Chem. A* **2019**, *7*, 23378−23415.
(31) Ryu, J.; Park, B.; Kang, J.; Hong, D.; Kim, S.-D.; Yoo, J.-K.; Yi, J. W.; Park, S.; Oh, Y. Three-Dimensional Monolithic Organic Battery Electrodes. *ACS Nano* **2019**, *13*, 14357−14367.
(32) Tie, Z.; Niu, Z. Design Strategies for High-Performance Aqueous Zn/Organic Batteries. *Angew. Chem., Int. Ed.* **2020**, *59*, 21293−21303.
(33) Das, S.; Heasman, P.; Ben, T.; Qiu, S. Porous Organic Materials: Strategic Design and Structure−Function Correlation. *Chem. Rev.* **2017**, *117*, 1515−1563.
(34) Buyukcakir, O.; Yuksel, R.; Jiang, Y.; Lee, S. H.; Seong, W. K.; Chen, X.; Ruoff, R. S. Synthesis of Porous Covalent Quinazoline Networks (CQNs) and Their Gas Sorption Properties. *Angew. Chem., Int. Ed.* **2019**, *58*, 872−876.
(35) An, Y.; Tan, S.; Liu, Y.; Zhu, K.; Hu, L.; Rong, Y.; An, Q. Designs and applications of multi-functional covalent organic frameworks in rechargeable batteries. *Energy Storage Mater.* **2021**, *41*, 354−379.
(36) Buyukcakir, O.; Ryu, J.; Joo, S. H.; Kang, J.; Yuksel, R.; Lee, J.; Jiang, Y.; Choi, S.; Lee, S. H.; Kwak, S. K.; Park, S.; Ruoff, R. S. Lithium Accommodation in a Redox-Active Covalent Triazine Framework for High Areal Capacity and Fast-Charging Lithium-Ion Batteries. *Adv. Funct. Mater.* **2020**, *30*, No. 2003761.
(37) Patel, H. A.; Hyun, J. S.; Park, J.; Chen, D. P.; Jung, Y.; Yavuz, C. T.; Coskun, A. Unprecedented high-temperature CO2 selectivity in N2-phobic nanoporous covalent organic polymers. *Nat. Commun.* **2013**, *4*, No. 1357.
(38) Xu, H.; Gao, J.; Jiang, D. Stable, crystalline, porous, covalent organic frameworks as a platform for chiral organocatalysts. *Nat. Chem.* **2015**, *7*, 905−912.
(39) Wang, S.; Li, H.; Huang, H.; Cao, X.; Chen, X.; Cao, D. Porous organic polymers as a platform for sensing applications. *Chem. Soc. Rev.* **2022**, *51*, 2031−2080.
(40) Li, Z.; Yang, Y.-W. Macrocycle-Based Porous Organic Polymers for Separation, Sensing, and Catalysis. *Adv. Mater.* **2022**, *34*, No. 2107401.
(41) Hu, Y.; Wayment, L. J.; Haslam, C.; Yang, X.; Lee, S.-h.; Jin, Y.; Zhang, W. Covalent organic framework based lithium-ion battery: Fundamental, design and characterization. *EnergyChem* **2021**, *3*, No. 100048.
(42) Ai, Q.; Fang, Q.; Liang, J.; Xu, X.; Zhai, T.; Gao, G.; Guo, H.; Han, G.; Ci, L.; Lou, J. Lithium-conducting covalent-organic-frameworks as artificial solid-electrolyte-interphase on silicon anode for high performance lithium ion batteries. *Nano Energy* **2020**, *72*, No. 104657.
(43) Zhang, C.; Lu, C.; Zhang, F.; Qiu, F.; Zhuang, X.; Feng, X. Two-dimensional organic cathode materials for alkali-metal-ion batteries. *J. Energy Chem.* **2018**, *27*, 86−98.
(44) Zhou, T.; Zhao, Y.; Choi, J. W.; Coskun, A. Lithium-Salt Mediated Synthesis of a Covalent Triazine Framework for Highly Stable Lithium Metal Batteries. *Angew. Chem., Int. Ed.* **2019**, *58*, 16795−16799.
(45) Wu, C.; Hu, M.; Yan, X.; Shan, G.; Liu, J.; Yang, J. Azo-linked covalent triazine-based framework as organic cathodes for ultrastable capacitor-type lithium-ion batteries. *Energy Storage Mater.* **2021**, *36*, 347−354.
(46) Amin, K.; Ashraf, N.; Mao, L.; Faul, C. F. J.; Wei, Z. Conjugated microporous polymers for energy storage: Recent progress and challenges. *Nano Energy* **2021**, *85*, No. 105958.
(47) Xu, F.; Chen, X.; Tang, Z.; Wu, D.; Fu, R.; Jiang, D. Redox-active conjugated microporous polymers: a new organic platform for highly efficient energy storage. *Chem. Commun.* **2014**, *50*, 4788−4790.
(48) Ghasemiestahbanati, E.; Shehzad, A.; Konstas, K.; Setter, C. J.; O'Dell, L. A.; Shaibani, M.; Majumder, M.; Hill, M. R. Exceptional lithium diffusion through porous aromatic framework (PAF) interlayers delivers high capacity and long-life lithium−sulfur batteries. *J. Mater. Chem. A* **2022**, *10*, 902−911.
(49) Zhao, S.; Bian, Z.; Liu, Z.; Wang, Y.; Cui, F.; Wang, H.-g.; Zhu, G. Bottom-Up Construction of Fluorene-Based Porous Aromatic Frameworks for Ultrahigh-Capacity and High-Rate Alkali Metal-Ion Batteries. *Adv. Funct. Mater.* **2022**, *32*, No. 2204539.
(50) Wang, W.; Kale, V. S.; Cao, Z.; Kandambeth, S.; Zhang, W.; Ming, J.; Parvatkar, P. T.; Abou-Hamad, E.; Shekhah, O.; Cavallo, L.; Eddaoudi, M.; Alshareef, H. S. Phenanthroline Covalent Organic Framework Electrodes for High-Performance Zinc-Ion Supercapattery. *ACS Energy Lett.* **2020**, *5*, 2256−2264.
(51) Wang, X.; Tang, J.; Tang, W. Manipulating Polymer Configuration to Accelerate Cation Intercalation Kinetics for High-Performance Aqueous Zinc-Ion Batteries. *Adv. Funct. Mater.* **2022**, *32*, No. 2200517.
(52) Wang, X.; Zhou, J.; Li, Z.; Tang, W. N-Heteroaromatic fused-ring cyanides extended as redox polymers for high rate capability aqueous zinc-ion battery. *J. Mater. Chem. A* **2023**, *11*, 2412−2418.
(53) Zhang, H.; Zhong, L.; Xie, J.; Yang, F.; Liu, X.; Lu, X. A COF-Like N-Rich Conjugated Microporous Polytriphenylamine Cathode with Pseudocapacitive Anion Storage Behavior for High-Energy Aqueous Zinc Dual-Ion Batteries. *Adv. Mater.* **2021**, *33*, No. 2101857.
(54) Peng, H.; Montes-García, V.; Raya, J.; Wang, H.; Guo, H.; Richard, F.; Samorì, P.; Ciesielski, A. Supramolecular engineering of cathode materials for aqueous zinc-ion hybrid supercapacitors: novel thiophene-bridged donor−acceptor sp^2 carbon-linked polymers. *J. Mater. Chem. A* **2023**, *11*, 2718−2725.
(55) Khayum M, A.; Ghosh, M.; Vijayakumar, V.; Halder, A.; Nurhuda, M.; Kumar, S.; Addicoat, M.; Kurungot, S.; Banerjee, R. Zinc ion interactions in a two-dimensional covalent organic framework based aqueous zinc ion battery. *Chem. Sci.* **2019**, *10*, 8889−8894.
(56) Ma, D.; Zhao, H.; Cao, F.; Zhao, H.; Li, J.; Wang, L.; Liu, K. A carbonyl-rich covalent organic framework as a high-performance cathode material for aqueous rechargeable zinc-ion batteries. *Chem. Sci.* **2022**, *13*, 2385−2390.
(57) Lin, Z.; Lin, L.; Zhu, J.; Wu, W.; Yang, X.; Sun, X. An Anti-Aromatic Covalent Organic Framework Cathode with Dual-Redox Centers for Rechargeable Aqueous Zinc Batteries. *ACS Appl. Mater. Interfaces* **2022**, *14*, 38689−38695.
(58) Zheng, S.; Shi, D.; Yan, D.; Wang, Q.; Sun, T.; Ma, T.; Li, L.; He, D.; Tao, Z.; Chen, J. Orthoquinone−Based Covalent Organic Frameworks with Ordered Channel Structures for Ultrahigh Performance Aqueous Zinc−Organic Batteries. *Angew. Chem., Int. Ed.* **2022**, *61*, No. e202117511.
(59) Wang, Y.; Wang, X.; Tang, J.; Tang, W. A quinoxalinophenazinedione covalent triazine framework for boosted high-performance aqueous zinc-ion batteries. *J. Mater. Chem. A* **2022**, *10*, 13868−13875.
(60) Wang, W.; Kale, V. S.; Cao, Z.; Lei, Y.; Kandambeth, S.; Zou, G.; Zhu, Y.; Abouhamad, E.; Shekhah, O.; Cavallo, L.; Eddaoudi, M.; Alshareef, H. Molecular Engineering of Covalent Organic Framework Cathodes for Enhanced Zinc-Ion Batteries. *Adv. Mater.* **2021**, *33*, No. 2103617.
(61) Ye, F.; Liu, Q.; Dong, H.; Guan, K.; Chen, Z.; Ju, N.; Hu, L. Organic Zinc-Ion Battery: Planar, π-Conjugated Quinone-Based Polymer Endows Ultrafast Ion Diffusion Kinetics. *Angew. Chem., Int. Ed.* **2022**, *61*, No. e202214244.
(62) Ouyang, Z.; Tranca, D.; Zhao, Y.; Chen, Z.; Fu, X.; Zhu, J.; Zhai, G.; Ke, C.; Kymakis, E.; Zhuang, X. Quinone-Enriched Conjugated Microporous Polymer as an Organic Cathode for Li-Ion Batteries. *ACS Appl. Mater. Interfaces* **2021**, *13*, 9064−9073.
(63) Peng, H.; Huang, S.; Montes-García, V.; Pakulski, D.; Guo, H.; Richard, F.; Zhuang, X.; Samorì, P.; Ciesielski, A. Supramolecular Engineering of Cathode Materials for Aqueous Zinc-ion Energy Storage Devices: Novel Benzothiadiazole Functionalized Two-

https://doi.org/10.1021/acsaem.3c01163
ACS Appl. Energy Mater. 2023, 6, 7672−7680

Dimensional Olefin-Linked COFs. *Angew. Chem., Int. Ed.* **2023**, *62*, No. e202216136.
(64) Shi, H.-Y.; Ye, Y.-J.; Liu, K.; Song, Y.; Sun, X. A Long-Cycle-Life Self-Doped Polyaniline Cathode for Rechargeable Aqueous Zinc Batteries. *Angew. Chem., Int. Ed.* **2018**, *57*, 16359−16363.
(65) Wang, X.; Wang, G.; He, X. Anthraquinone porous polymers with different linking patterns for high performance Zinc-Organic battery. *J. Colloid Interface Sci.* **2023**, *629*, 434−444.
(66) Wang, J.; Liu, Z.; Wang, H.-g.; Cui, F.; Zhu, G. Integrated pyrazine-based porous aromatic frameworks/carbon nanotube composite as cathode materials for aqueous zinc ion batteries. *Chem. Eng. J.* **2022**, *450*, No. 138051.
(67) Huang, L.; Li, J.; Wang, J.; Lv, H.; Liu, Y.; Peng, B.; Chen, L.; Guo, W.; Wang, G.; Gu, T. Organic Compound as a Cathode for Aqueous Zinc-Ion Batteries with Improved Electrochemical Performance via Multiple Active Centers. *ACS Appl. Energy Mater.* **2022**, *5*, 15780−15787.
(68) Yue, X.; Liu, H.; Liu, P. Polymer grafted on carbon nanotubes as a flexible cathode for aqueous zinc ion batteries. *Chem. Commun.* **2019**, *55*, 1647−1650.
(69) Wang, J.; Polleux, J.; Lim, J.; Dunn, B. Pseudocapacitive Contributions to Electrochemical Energy Storage in TiO2 (Anatase) Nanoparticles. *J. Phys. Chem. C* **2007**, *111*, 14925−14931.
(70) Li, Z.; Tan, J.; Zhu, X.; Xie, S.; Fang, H.; Ye, M.; Shen, J. High capacity and long-life aqueous zinc-ion battery enabled by improving active sites utilization and protons insertion in polymer cathode. *Energy Storage Mater.* **2022**, *51*, 294−305.

https://doi.org/10.1021/acsaem.3c01163
ACS Appl. Energy Mater. 2023, 6, 7672−7680